JOURNAL OF MATERIALS RESEARCH AND TECHNOLOGY 2022;17:2725–2741

Available online at www.sciencedirect.com

jmr&t Journal of Materials Research and Technology

journal homepage: www.elsevier.com/locate/jmrt

Original Article

The effect of preforming and infusing bindered and unbindered carbon non-crimp-fabrics on the final quality of composites parts

N.G. Pérez-de-Eulate [a,*], N. Ortega [b], I. Holgado [c], F.J. Vallejo [a], S. Moralejo [a], P. Olaskoaga [a]

[a] IDEKO, Arriaga Industrialdea, 2, E-20870, Elgoibar, Spain

[b] Department of Mechanical Engineering, University of the Basque Country (UPV/EHU), Alameda de Urquijo S/n, 48013, Bilbao, Spain

[c] CFAA—University of the Basque Country (UPV/EHU), Parque Tecnológico de Zamudio 202, 48170, Bilbao, Spain

ARTICLE INFO

Article history:
Received 25 October 2021
Accepted 2 February 2022
Available online 9 February 2022

Keywords:
Non-crimp fabrics
Preforming
Resin infusion
CT

ABSTRACT

Vacuum infusion (VI) is a liquid moulding process used to manufacture fibre-reinforced polymer composite parts. The VI process for non-crimp fabric (NCF) preforms is one of the most promising processes for improving the quality and cost efficiency of traditional processes using prepregs and autoclave curing. An understanding of the preform thickness behaviour in the compaction, wetting, and curing stages is necessary to optimise the overall process and obtain high-performance composite parts. In this study, the influence of the material, preforming, and infusion parameters on the thickness of four different carbon NCF laminates were investigated. The preforming behaviour includes the influence of the NCF composition, such as the presence of an organic binder or the number of compaction steps. Infusion was characterised using dielectric analysis (DEA). The properties of the resulting composites were analysed in terms of the fibre volume fraction (FVF) and porosity, as measured using X-ray computed tomography (CT). The main consequence of the outcome of the present study is that, from a manufacturing point of view, downward through-thickness resin infusion offers benefits in terms of thickness, FVF, and porosity tolerance. In addition, the acquired results allow for the identification of the main settings for an optimised consolidation strategy, which could be used for manufacturing NCF composite parts.

1. Introduction

The composite industry has been striving to find more cost-effective manufacturing processes than those based on autoclaves. Current processes based on automatic tape lay-up (ATL) and automatic fibre placement (AFP) for thermoset prepregs and autoclave curing are not sufficient to meet current and future cost requirements, especially in the aerospace

* Corresponding author.
E-mail address: ngutierrez@ideko.es (N.G. Pérez-de-Eulate).

https://doi.org/10.1016/j.jmrt.2022.02.007

industry [1]. This is mainly due to the costs associated with the need to store prepregs at −18 °C, the rate of the lay-up process (limited to 20 kg/h), and the high cost of autoclave curing.

One of the most promising cost-effective manufacturing strategies is the automated lay-up of dry carbon non-crimp fabrics (NCFs) followed by the VI process [2], where the costs incurred by the vacuum-bag assembly process are lower compared to the cost associated to the autoclave processes [3]. As a substitute for prepregs, NCFs have become one of the most relevant dry textiles for providing reinforcement. NCFs are defined as multiaxial fabrics, fixed by warp-knitting [4] frequently with small amounts of binders on the surface. Binders are solid-state polymer adhesives that need to be melted to bond the individual fabric layers together during the preforming [5], allowing the preform to be handled without damaging the dry fibres [6,7]. The automatic lay-up of NCFs has been the subject of development over the last decade. Robotic pick and place NCF lay-up systems are limited to small- or low-volume production, such as the placement of patches, and the placement of one layer on a previously consolidated laminate [8–10]. Other technologies offer the possibility of laying up NCFs without binder activation, thus increasing the lay-up rates up to 10 times [8,11] compared to dry fibre placement (DFP) technology [12,13]. DFP is the most mature dry fibre tow laying-up technology. DFP technology requires that the binder be melted to hold the layers together during the laying-up. This requires the use of a heating system [14], resulting in a greater consumption of resources and time [7].

The VI process avoids the need for autoclaving and decreases the tooling cost [15,16]. Other benefits of the use of VI in the manufacturing of integrated structures are the reduction in assembly time, good dimensional conformity, minimal or no shimming, a better non-destructive inspection pass rate, and minimal material spring-back [2].

Resin infiltration occurs after the dry reinforcement lay-up, producing a preform [17]. The compaction of the preform has a significant influence on the resin infiltration and the control of the thickness of the final composite part. Thus, if the infused volume is greater than the volume required for dry lamination, due to over- or under-compaction, the fibre volume fraction (FVF), and consequently the thickness and quality of the final composite part will be less than optimal [18]. Hence, knowledge of the compaction behaviour of the preform is of utmost importance to ensure the optimum quality of a composite part.

With the goal of being able to control this process, several studies have focused on controlling the thickness of the different sub-processes, such as the dry compaction, fibre settlement, and relaxation of the fibres [19–22]. The main conclusion drawn is that dry laminate compaction does not significantly influence the final FVF compared to wet laminates [23], whereby, to reach the desired FVF, several compaction cycles are necessary; therefore, the preforming time is considerably increased [24]. There is much less relaxation of the fibres during decomposition than that during the compaction and settling. This indicates that fabric specimens are not elastic materials, but viscoelastic; therefore, over time, the relaxation is strongly dependent on the initial compression and fibre alignment [25].

The binder and its process parameters also play an important role in controlling the thickness. Recent investigations [26–28] point to the influence of the binder (type, quantity, temperature, and activation time) as being critical factors that are directly related to the behaviour of NCF materials during compaction.

Regarding resin infiltration by the VI process, the configuration of the vacuum bag system, which is composed of different auxiliary materials, significantly affects the properties of the final composite part. The various VI methodologies each have their own advantages and disadvantages [3,29–34]. One recent and promising infusion process is the vacuum-assisted process (VAP ®), which is patented by Airbus. This process has the following advantages [17,35]: (i) continuous purging of air/gas trapped in the laminate through a semi-permeable membrane (permeable to gas, but not to resin) in the through-thickness direction, while trapping the resin, and (ii) maintenance of a constant vacuum pressure throughout the preform. In other infusion processes such as Seemann's composite resin infusion moulding process (SCRIMP™), vent ports are located such that the flow front of the resin arrives there last, and the impregnated laminates must undergo decompactions to remove air trapped within them. In contrast, in the VAP method, this is not necessary because the air is evacuated over the entire vacuum infusion area [36]. Regarding other composite materials and manufacturing processes, researchers consider the effect of internal porosity as an important factor to reduce defects and increase the compactness of the materials, thus improving the bond strength between the composite components [37]. Furthermore, with respect to bond strengths, it was reported that by coating carbon fibre with e.g. PyC/SiC composite in carbon fibre reinforced aluminium (Cf/Al) composites [38], the compatibility between fibres and matrix was improved by changing the wettability and controlling the interface, which could be analogous to the presence of binder in carbon fibre NCFs.

For the above reasons, this study aimed to investigate the preform compaction and resin infiltration behaviours of vacuum-infused carbon NCF composites. The study examined the influence of the material and process parameters on the compaction and resin infiltration of four carbon NCF laminates, namely, NB (laminate without binder), BNC (laminate with binder but not compacted), BC (laminate with binder, compacted in one step), and BC_{5S} (laminate with binder, compacted over five steps). These laminates were selected to analyse the influence of the presence of binder and the compaction process on the quality of the final composite part. The properties of the resulting composites were analysed in terms of thickness, FVF, and porosity using X-ray computed tomography (CT).

2. Materials and experimental procedure

2.1. Materials

In this study, two biaxial reinforcements, 0/90° and 45°/-45°, based on carbon NCFs were used (Saertex GmbH & Co. KG). Bindered and unbindered NCFs were studied. The bindered

Table 1 – Material specifications.

Material	Material type	Fibre Orientation (°)	Areal density (g/m^2)	Binder Presence
Reinforcement	High strength/standard modulus aerospace-grade carbon fibres	0/90	565	Yes
		45/-45	548	Yes
		0/90	557	No
		45/-45	540	No
Binder	Thermoplastic resin	–	8	–
Yarn	Polyester	–	6	–

contained the Epikote Resin 05311 binder, which is a thermoplastic polymer based on bisphenol-A and marketed by Hexion Specialty Chemicals. The type of reinforcement, fibre orientation, areal density, type and the presence of binder, and the yarn used for the stitching of the layers are listed in Table 1. For the bindered fabrics, the powder binder was located only on the rear face of the fabric. Figure 1 shows magnified images of each fabric, illustrating the presence or absence of a binder on each face.

For the infusion process, SR 8100 epoxy resin and SD 8823 hardener were used (Sicomin Epoxy Systems). To remove any bubbles from the resin, it was degassed for 24 h before being injected into the preform, after which it was cured at room temperature. The mixture was degassed in a pressure vessel for 5 min. The resin viscosity at 25 °C was 785 ± 155 mPa s, and the gel time was set to 3 h 45 min [39].

2.2. *Experimental procedure*

2.2.1. *Preforming*

Table 2 describes the laminates used in this study, each of which consisted of 20 layers of carbon NCFs laminated in a $[45/-45/0/90]_{10}$ configuration, each measuring 150 × 150 mm. The amount of binder in the bindered laminates corresponded to 1.4% of the total weight. All cut and stacked specimens were stored for at least 24 h to allow the release of the deformation induced by the cutting process. Four different laminate configurations were used. These were classified as unbindered (No Binder (NB)) and bindered samples (Binder No Compacted (BNC), Binder Compacted in one step (BC), Binder Compacted in five steps (BC_{5S})). The terminology "steps" is used to describe the process of preforming. One-step compaction involves preforming a symmetrical laminate of 20 layers in one step under vacuum and pressure; however, five-step compaction means preforming the compaction of the laminate every four layers up to a total of 20 layers, resulting in five consecutive stepwise vacuuming and pressuring steps.

For BC and BC_{5S}, the compaction temperature must exceed the binder activation temperature. Hence, the glass transition temperature (T_g) of the binder was determined using differential scanning calorimetry (DSC). The obtained value was set to $T_g = 76 \pm 5$ °C at 10 °C/min. Thus, 110 °C was applied in the compaction experiments to ensure complete softening of the binder.

The systematic preforming experiments were conducted using hot drape forming (HDF) equipment (Global Vacuum Presses), provided with a 2 mm flexible silicone membrane, suitable for the application of vacuum pressure (1 bar) over a wide range of temperatures. The binder was thermally activated using the heating resistances.

In line with the results of previous studies [23,28], to characterise the influence of the preforming process on laminate thickness, the experiments were divided into two main stages: compression and recovery. Compression entails compaction (under 110 °C and vacuum pressure for 2 h) and settling (under 25 °C and vacuum pressure, until stabilisation is attained), whereas the recovery stage includes decompaction (where the vacuum pressure is released) and

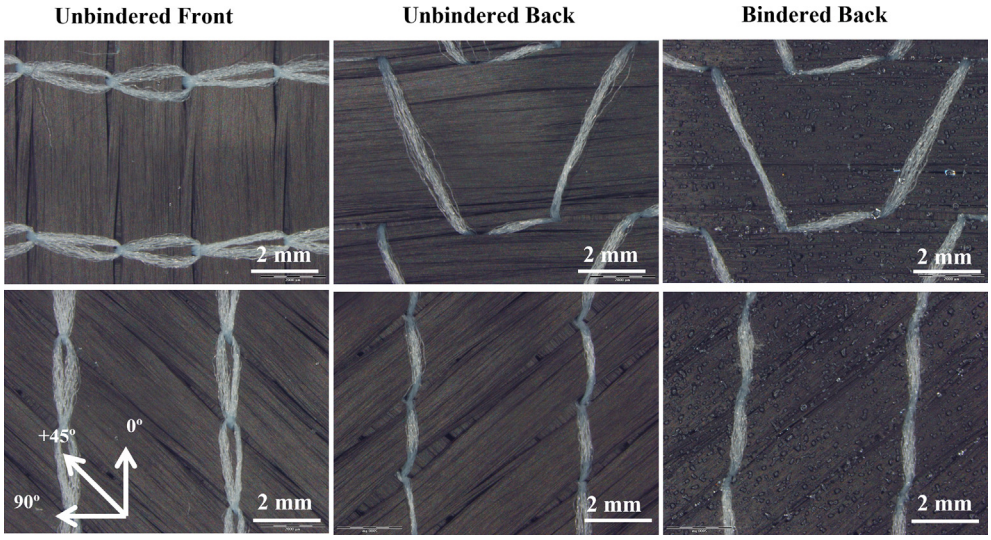

Fig. 1 – Magnified images of carbon fibre NCFs, displaying front and rear faces of the unbindered and bindered samples.

Table 2 – Sample description and preforming conditions for hot drape forming (HDF).

Class	ID Laminate	Description	Compression conditions	
			Steps	Temperature (°C)
Unbindered	NB	No Binder	1	25
Bindered	BNC	Binder No Compacted	–	–
	BC	Binder Compacted in 1 Step	1	110
	BC_{5S}	Binder Compacted in 5 Steps	5	110

relaxation. All the experiments were performed using flat specimens to eliminate the influence of the fabric shear behaviour. Figure 2 illustrates the thickness monitoring response.

2.2.2. *Infusion process*

For the infusion process, each fibre preform was placed between a rigid lower mould half and a vacuum bag functioning as the upper mould half. In this study, three different resin flow directions (Z_{down}, Z_{up}, XYZ) were tested. Figure 3 shows the vacuum infusion setup. For the infusions in the Z-direction, the process was based on the Airbus VAP® process [34]. The resin flow direction was controlled by a semipermeable microporous membrane, which was placed upwards and downwards in the infusion vacuum bag configuration, indicated as Z_{up} and Z_{down}, respectively. The semipermeable membrane was Dahltexx® SP-2 (Airtech). For the in-plane and through-thickness directions, the process was based on the SCRIMP™ process. The resin was transferred to the XYZ plane without a semipermeable membrane. Nonetheless, a small piece of the membrane was placed over the vacuum port to prevent the entrance of the resin.

After the preparation of each vacuum bag configuration, all the laminates were kept under a pressure of 1 bar for 30 min to avoid possible relaxation of the specimens [40] and to promote the settlement of the fibres [20]. Span pressure sensors (Festo) were used to monitor the leakage of pressure during the process.

The flow behaviour and curing of the resin/hardener mixture were monitored using dielectric analysis, in which the ionic viscosity data were obtained using a DEA 288 Epsilon dielectric analyser (Netzsch) equipped with specific sensors for carbon. The flow behaviour during the entire infusion was monitored in situ by introducing disposable dielectric sensors into the bottom (Z_{down} and XYZ) or top (Z_{up}) of each laminate.

Dielectric analysis (DEA) can be used to analyse the curing behaviour of composites by applying a voltage from an electrode sensor placed in contact with the matrix resin. The time-varying voltage was applied over a wide range of frequencies (1 kHz, used in the present study). The change in the amplitude and phase angle shift in the signal relative to the applied voltage was measured and used to calculate the dielectric properties of the resin, such as dielectric constant (permittivity), dielectric loss factor, ionic conductivity (σ), and ionic viscosity (ρ), that is, the electrical resistivity. As the resin changes from a liquid to a solid, the amount and mobility of charged ions both decrease because of the growing molecular network. The electrical resistivity or ionic viscosity (ρ) is calculated directly as the inverse of the conductivity (σ) of the resin using the following relationship: $\rho = 1/\sigma$.

DEA involves measuring changes in the dielectric properties of a material by using an impedance analyser over many frequencies. Dielectric cure monitoring is sensitive to the mobility of ions and the rotational mobility of dipoles on a polymer molecule in the presence of an electric field [41]. The experiments were conducted using disposable interdigitated electrode sensors (IDEX) inserted directly into the vacuum infusion configuration, as described in the previous section. In the present study, the resin curing behaviour was monitored according to the evolution of the ionic viscosity over time.

2.3. *Characterization techniques*

The thickness of the carbon fibre laminates was measured using a laser displacement sensor. The experimental setup consisted of a laser displacement sensor (Sick), with a measuring range of 300–700 mm and a wavelength of 658 nm and a thermocouple (Tc Direct), where controlled by a programmable controller (PLC) (B&R) connected to a computer. Data acquisition was performed at 1 s intervals and exported every 10 min. Figure 4 shows the compression and recovery stage setup.

The fibre volume fraction (FVF) of the specimens was determined by acid digestion according to the protocol described in the ASTM D3171-15 standard [42], using nitric acid 69% ACS ISO (Panreac®). The resin (ρ_r) and composite (ρ_c) densities were calculated using the immersion method described in UNE-EN ISO 1183–1:2019 [43], set at a constant value of 1.18 g/cm^3 for the resin. For composite densities, there was a variation in the value depending on the conditions. The volumetric density of the fibre was provided by the supplier (1.77 g/cm^3). The experimental porosity (V_0) was calculated using Eq. (1) according to UNE-EN 2564:2018 [44].

$$V_0 = 100 - \left[W_f \frac{\rho_c}{\rho_f} + (100 - W_f) \frac{\rho_c}{\rho_r} \right] \quad (1)$$

where W_f is the fibre content by mass, obtained by acid digestion; ρ_c, ρ_f, and ρ_r are the densities of the composite, fibre, and resin, respectively.

X-ray computed tomography (CT) was used as a non-destructive method. CT allows us to obtain images of the interior of the whole part and observe possible changes in the density as an indicator of the existence of defects. To do this, a General Electric X-Cube Compact machine was used. Defects in the reconstructed object were qualitatively analysed using VGStudio MAX 3.4 software using the porosity and inclusion analysis module. The maximum voltage and current of the CT system were 195 kV and 8 mA, respectively. The focus size was 0.4/1 mm.

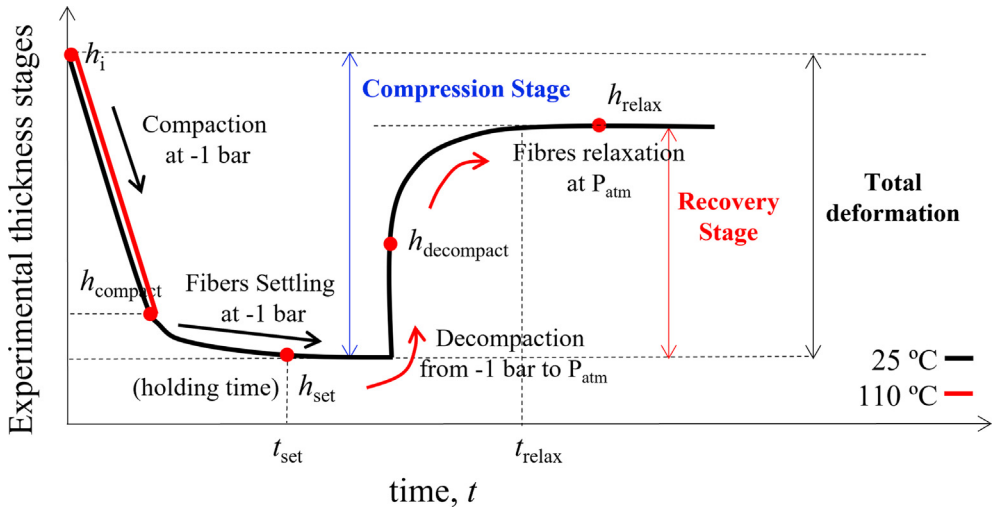

Fig. 2 – Thickness response during compression and recovery stages as a function of time [23,28].

Voltage and current are the most influential input parameters affecting the scanning quality. Taking this into account, the voltage was set to 192 kV whereas the tube current was adjusted to be high enough to minimize the exposure. The tube current was 2 mA and the exposure time, 100 ms. The homogenisation of the photon energy of the beam was performed through the combination of 1-mm copper and 0.5-mm tin filters. All scanned samples were scanned under the same scan conditions and orientations into the machine. The resulting voxel size was 152 μm. The samples were fixed in a 3-jaw chuck and loaded into the machine as shown in Fig. 5.

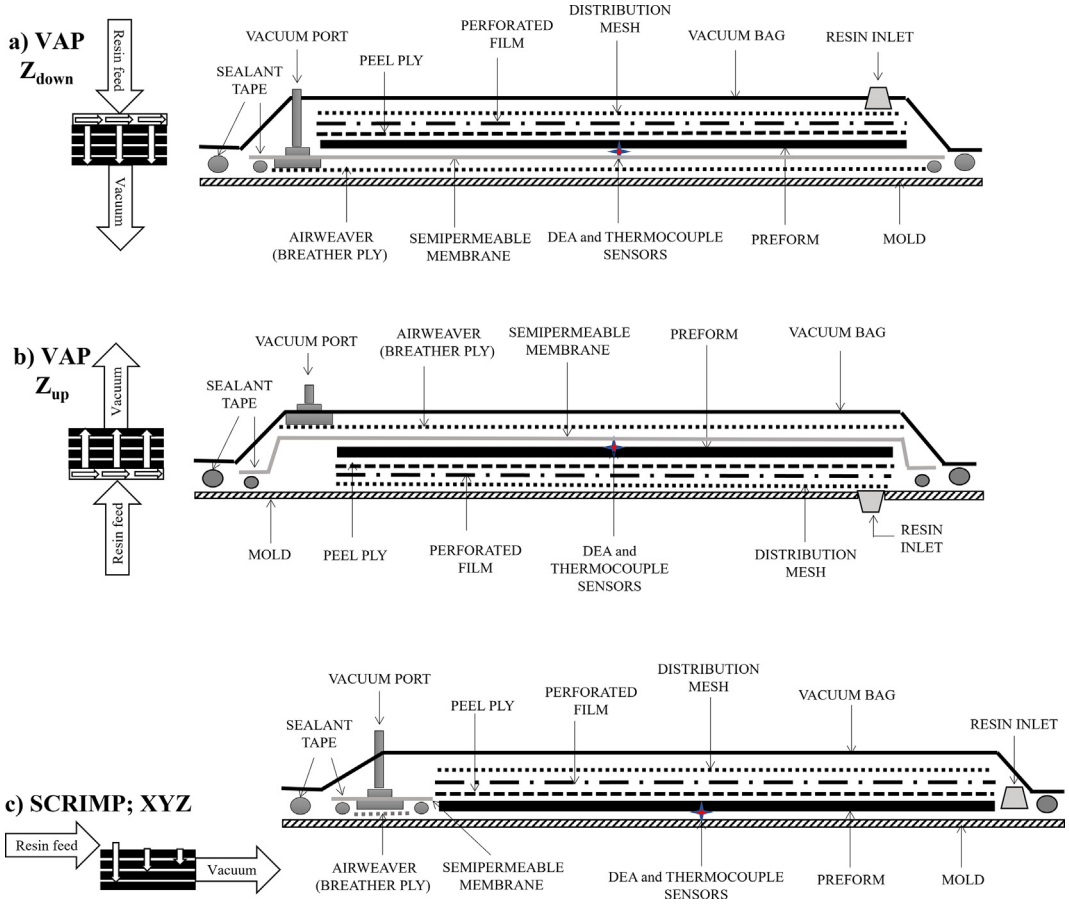

Fig. 3 – Infusion configurations with different flow directions (a) Z_{down} (b) Z_{up} (c) XYZ.

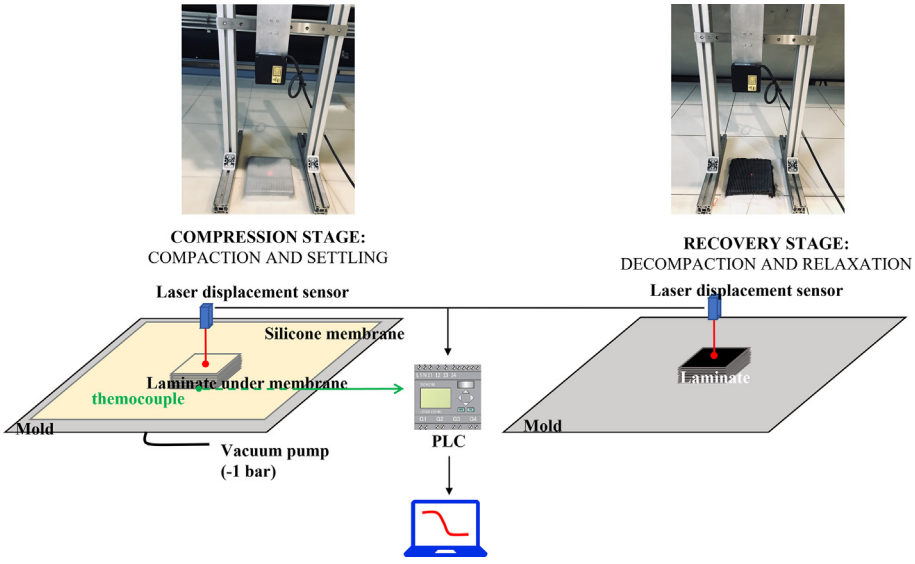

Fig. 4 – Thickness monitoring using laser displacement sensor.

3. Results and discussion

3.1. *Preforming process: compression and recovery stages*

The effect of compaction and the presence of binder on the carbon NCF laminate thickness were studied in the preforming experiments by measuring the thickness using a laser displacement sensor. The reproducibility of the results was investigated by examining five samples of each laminate (NB, BNC, BC, and BC_{5S}) in parallel. The error bars represent the standard deviation of five samples belonging to each laminate group. Figure 6 is an overview of the thickness variation during compaction, settling, decompaction, and relaxation as a function of time. The thicknesses of the studied laminates at all stages are listed in Table 3. Note that, for the compaction, two different temperatures were employed: a high temperature (110 °C) for activating the binder in the BC and BC_{5S} samples, and room temperature (RT = 25 °C) for NB and BNC, that is, the unbindered and unmelted bindered samples, respectively. For the BC and BC_{5S} samples, the compaction stage lasts 7200 s, which is the time required to heat the samples to 110 °C and reach a stable temperature. Therefore, provided that the compaction pressure is the same for all the samples, the binder activation temperature has more influence in the compaction behaviour rather than the number of compaction cycles or steps exerted, for instance, for BC_{5S} laminates. Irrespective of the number of plies, different settling times were achieved depending on the preforming process, which is the preferred strategy responsible for the major compaction and settling times. The settling time was defined as being dependent on the nature of the reinforcement, that is, depending on the presence or activation of the binder system.

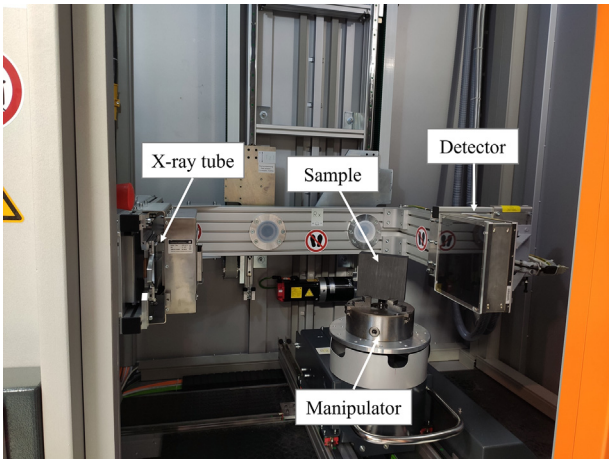

Fig. 5 – Sample to be scanned into CT machine.

The initial thickness of the NB laminates (16.28 ± 0.36 mm) was slightly greater than those obtained for the BNC, BC, and BC_{5S} laminates (16.07 ± 0.38, 16.05 ± 0.5 and 16.03 ± 0.52 mm, respectively). The initial thickness was measured after the air removal. This process consisted of a 5-min pressurisation with a silicone membrane at 1 bar and RT. The slight difference between the NB laminate (without binder) and the other laminates (with binder) is due to the tacky nature of the binder, which lightly affixes one layer to another, giving rise to laminates with less thickness when the pressure is released.

When pressure (1 bar) and heat (110 °C) were applied, the thickness decrease was similar in the BC and BC_{5S} laminates and lower for the NB and BNC laminates, with BNC exhibiting the smallest decrease. Binder activation in the compaction step at 110 °C under a vacuum leads to the re-organization of the fibres, which is facilitated by the lubricating effect of the melted binder [45]. The BNC laminates exhibit less of a reduction because of the inactivated layer of the binder, which hinders the reorganisation of the fibres [27,28].

The settling stage is the time required to avoid thickness variations under a vacuum at RT. Table 3 shows that the thicknesses at the settling stage are slightly lower than those

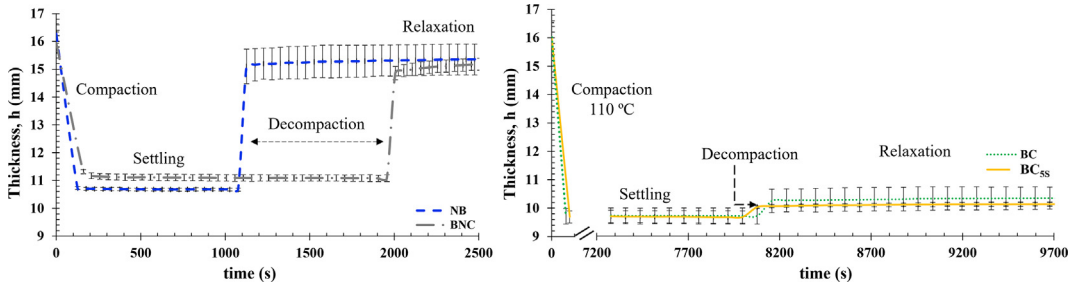

Fig. 6 – Thickness evolution versus time in compaction, settling, decompaction, and relaxation. Left panel: Compaction of NB and BNC at 25 °C. Right Panel: Compaction of BC and BC_{5S} at 110 °C. Settling, decompaction, and relaxation at 25 °C. The standard deviation of the five samples is represented by the error bars.

at the compaction stage in all the laminates, but the time needed to achieve these thickness values was higher in the BNC laminates than in the rest of the laminates (Fig. 6), because of the viscous nature of the unmelted binder. Compressing carbon NCFs at RT [40], preform thickness may still decrease with time because of the viscous behaviour as the pressure is constant. In the settling step, laminates are more compressed because fibres and tows slide into each other and stack more freely, creating a nesting effect, and the deformation behaviour is mainly viscous [23]. Nevertheless, the reduction in thickness in all the studied samples did not exceed 2% between the compaction and settling stages, making the settling stage avoidable in terms of manufacturing process.

In the recovery stage (decompaction and relaxation), the NB and BNC samples recovered most of their initial thickness due to the lack of or inactivation of the binder system, provoking the freedom of the fibres or tows to continue relaxing over time. In the relaxation step of the BNC samples, the change in the thickness was higher than in the remainder of the laminates, this being attributable to the inactivated powder binder in the NCF layers, which contributes to increasing the viscous effects in the relaxation process. On the other hand, the thicknesses of BC and BC_{5S} recover less than 1 mm, displaying dimensional stability due to the activation of the binder during compaction at high temperatures.

The preforming experiments show that the compression of a fabric preform is time-dependent under a constant load (under a vacuum), and by extending the compression and recovery stages to several hours, a steady state of carbon NCF laminates can be achieved. Regarding the NCF laminates, the results indicate that, regardless of the number of compaction steps to which the laminates are subjected, as long as the binder activation temperature is overcome under vacuum pressure, fully compressed laminates are obtained. The settling stage defines the steady-state thickness of the specimen, which is set as the initial thickness before resin infusion for dry NCF laminates.

3.2. *Infusion and post-infusion processes*

3.2.1. *"Effective" permeability and curing analysed by DEA*

Figure 7 shows as an example BNC composite part after resin infusion following the three flow directions (Z_{down}, Z_{up}, and XYZ) at RT. Incomplete fillings were found in all the laminates (NB, BNC, BC, and BC_{5S}) after being infused in the XYZ direction, which simulates the SCRIMP process. A previous study found that the resin flow on the surface is mainly governed by the permeability of the distribution medium [35]. In the present study, the main difference between the XYZ and Z directions is the use of the semi-permeable membrane. According to Li et al. [35], through-thickness resin infusions lead to a lower resin wastage, more uniform thicknesses, and fibre distribution, whereas in the SCRIMP infusion process, the location of the vent and the permeability of the reinforcement are critical, and could result in incomplete fillings.

With the XYZ resin infusion direction, the composite part filling occurs when the inlet line is closed and the excess resin present in the mould flows toward the reinforcement and the outlet, where the pressure equalisation takes place and the infusion is completed. The outlet is closed after gelation of the resin when the flow is no longer possible. The lack of filling is not only related to the resin viscosity, but also to the vacuum of the entire system. Given that the process can take several hours (the gel time of the resin is greater than 2 h at RT), if there

Table 3 – Thicknesses and standard deviation of studied laminates at all stages.

Stage	Thickness (mm)			
	NB	BNC	BC	BC_{5S}
Initial	16.28 ± 0.36	16.07 ± 0.38	16.05 ± 0.50	16.03 ± 0.52
Compaction	10.73 ± 0.15	11.31 ± 0.21	9.81 ± 0.24	9.76 ± 0.25
Settling	10.61 ± 0.17	11.13 ± 0.21	9.77 ± 0.24	9.71 ± 0.26
Decompaction	14.97 ± 0.74	14.34 ± 0.58	9.97 ± 0.24	10.04 ± 0.33
Relaxation	15.37 ± 0.67	15.35 ± 0.49	10.12 ± 0.20	10.17 ± 0.30

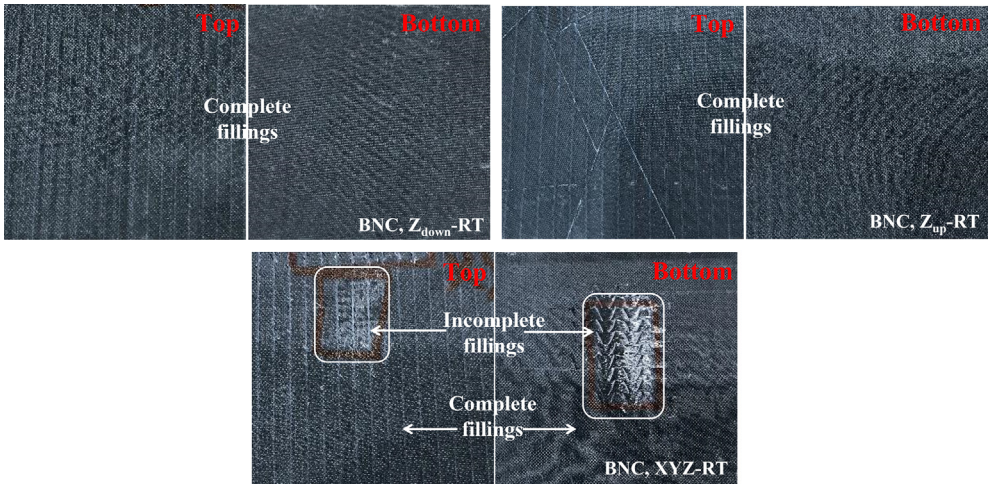

Fig. 7 – Top and bottom surface of infused BNC specimens at RT for the three studied flows (Z_{down}, Z_{up}; and XYZ).

is any leakage of the vacuum in the vacuum bag set-up, dry spots are likely to occur. Nevertheless, the VAP® process provides a uniform pressure throughout the process, implying that the VAP® is a more robust filling process capable of manufacturing composite parts with a greater thickness and a low risk of dry spot formation. Hence, to ease fibre impregnation in the in-plane and through-thickness directions (XYZ), the viscosity of the resin was modified by raising the temperature to 40 °C to enable the manufacture of fully wetted parts.

Figure 8 shows the resin arrival time as a function of time, represented by the logarithms of the ionic viscosity at 1 Hz for all the infused samples and flow directions. Data were obtained from the opening of the resin inlet to the arrival time of the resin to the detector, which is located on the opposite face to that of the resin inlet in the middle of the preform (see Fig. 3).

The arrival of the resin was detected because of the drastic drop in the logarithm of the ionic viscosity value, compared to that of the free carbon fabric. It is characterised by the onset of a drop. Owing to the resin and air having different dielectric constants, the dielectric sensor enables the measurement of the resin arrival as the capacity changes. Several studies not only reported the use of embedded optic fibres to monitor the resin infiltration in the composite reinforcement [46,47] but also used dielectric measurements to validate the optic fibre data [48]. Table 4 lists the resin arrival times.

The time values at the drop indicate the time required for the resin flow to travel from the vessel to the detector, which could be regarded as being an "effective" permeability measurement, defined as the average in-plane and through-thickness permeability value without accounting for the change in the thickness during the filling process [49]. This characterisation method ignores the change in the volume fraction and assumes that the permeability remains constant as the flow propagates.

Table 4 shows that the time required for the resin to travel from the inlet to the detector of the BNC laminates for the Z_{down} flow direction is higher (195 s) than that for the NB, BC, and BC_{5S} samples (120, 80, and 100 s, respectively). This indicates that the presence of an unmelted binder between the carbon fibre layers hinders the resin flow. This is in good agreement with the results of previous studies [50]. Even though it has been reported that soluble binders can increase the resin viscosity and prevent the filling of the mould [51], in the present study the compatibility of the employed binder and the resin was found to improve the "effective" permeability of the laminates. The times obtained for the bindered melted laminates such as BC and BC_{5S} (80 and 100 s, respectively) are lower than those for the NB laminates (120 s). Table 4 also summarizes that the times required for the resin to travel from the inlet to the detector for the NB and BNC laminates infused with the Z_{up} flow direction are significantly lower than those obtained for the NB and BNC laminates infused with the Z_{down} flow direction. This "effective" permeability difference could be a consequence of the different configuration set-ups for the Z_{down} and Z_{up} flows. Figure 3 shows the Z_{down} configuration setup, where the distribution mesh is in contact with the vacuum bag, and the Z_{up} configuration setup, where the distribution mesh is in contact with the metallic mould. For the Z_{down} flow, the vacuum bag could penetrate the unit cells of the distribution media under external pressure. This penetration significantly changes the overall permeability of the system [52]. This effect does not occur when the surface in contact with the distribution mesh is a rigid surface; therefore, in this case, the permeability of the distribution mesh is higher. This effect is not so clear when comparing BC and BC_{5S} laminates with the Z_{down} and Z_{up} flows because of the lower permeability of the compacted laminates.

Finally, the "effective" permeability in the XYZ direction of all the laminates was found to exhibit similar orders of magnitude as for that for the Z-direction resin infusion, even though the viscosity of the resin was lowered by the resin infusion at 40 °C, except for the BNC (Z_{down}) infusion. The in-plane and through-thickness "effective" permeability are caused by different mechanisms, as reported by Drapier et al. [53], whereby the through-thickness permeability of the non-crimp stitched fabrics was dominated by gaps created around

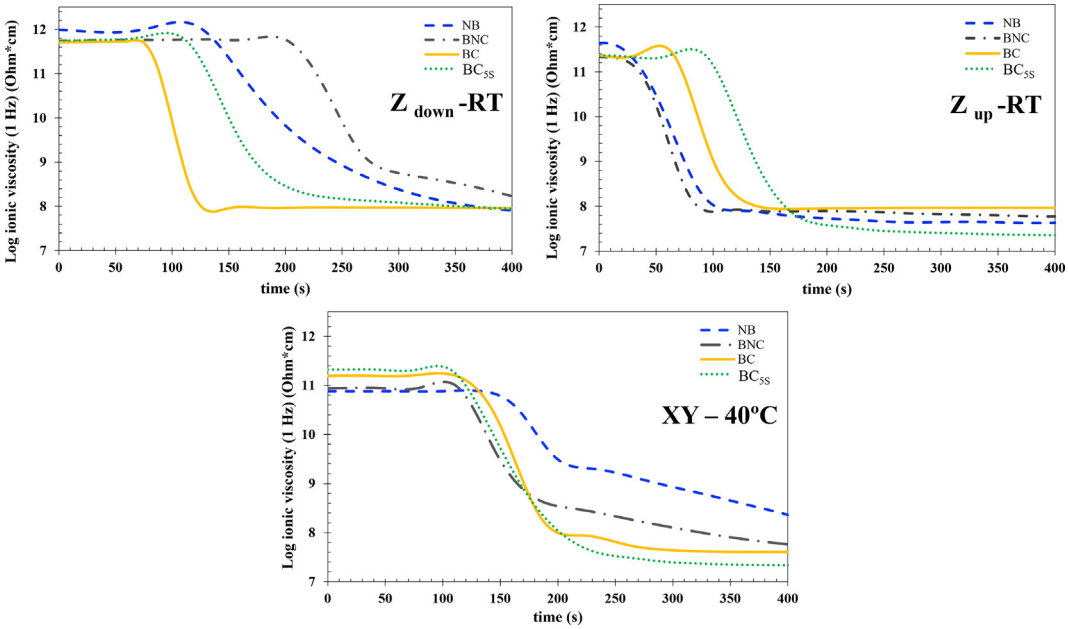

Fig. 8 – Logarithm of ionic viscosity from resin inlet opening to reaction start.

the stitches. This suggests a high sensitivity to the continuity of the gaps through the specimen thickness, but no sensitivity to the actual fibre arrangement. Hence, the through-thickness direction is set as the preferential resin flow path (path of least resistance), where the resin flow presents less hindrance.

Fig. 9 a), b), and c) show the curing behaviours of all the laminates with the different resin flow directions. The reaction conversion is assumed to be 0% when the ionic viscosity is a minimum, and 100% when the ionic viscosity is constant. Thus, based on the ionic viscosity curves, the time-dependent curing degree [$\alpha(t)$] of the composite parts was calculated using Eq. (2), where η_t is the ionic viscosity at time t, η_0 is the initial viscosity of the resin, and η_∞, is the maximum ionic viscosity of the resin [54], to examine the curing behaviour of each sample.

$$\alpha(t) = (\log \eta_t - \log \eta_0) / (\log \eta_\infty - \log \eta_0) \quad (2)$$

Hence, laminates formed with the XYZ flow direction require 30,000 s to reach 100% curing, whereas with the Z_{down} and Z_{up} flows, total curing is achieved after 36,000 s. This curing time acceleration with the XYZ flow direction is a result of the increase in the temperature during the resin infusion. In addition, Fig. 9 d) shows the reaction kinetics calculated from the slope of the curves. Comparing the reaction slopes for the Z_{down} and Z_{up} flows, there are no marked differences in the kinetics of the resin reaction among the different laminates (NB, BNC, BC, and BC_{5S}) to determine the existence of different reaction kinetics due to the presence or absence of binder, unlike what was observed for other types of reactive binders [55,56].

Table 4 – Arrival time at detector for all laminates and all three studied flows.

Laminate	Time from inlet to detector (s)		
	Z_{down}	Z_{up}	XYZ
NB	120 ± 6	16 ± 3	140 ± 8
BNC	195 ± 7	18 ± 3	120 ± 7
BC	80 ± 4	65 ± 3	115 ± 7
BC_{5S}	100 ± 5	95 ± 7	115 ± 5

3.2.2. *Thickness control*

Figure 10 displays the laser pattern for the thickness measurement and the thicknesses for all the infused laminates (NB, BNC, BC, and BC_{5S}) for the Z_{down} (a), Z_{up} (b), and XYZ (c) flow directions, before and after infusion. The thicknesses before infusion correspond to the values obtained after settling to avoid the relaxation effects of the laminates, as explained in the experimental section related to the infusion process. Figure 10 shows the sample thickness change from the dry laminate (after settling) to the composite part (after infusion) as a function of the resin infusion flow direction. For the BC and BC_{5S} laminates, the degree of compaction achieved in the settling process was lost after infusion in all the studied flow directions. For the no compacted laminates, i.e. NB and BNC, the thickness of the composite part increased with Z_{up} (4%) flow direction, given the higher permeability caused by the flatness of the distribution media, which allows achieving a higher permeability. Consequently, there is an increase in the final thickness of the composite part.

Owing to the use of the VI process, the resin flows through the fabric preform to relax the fabric, reducing its compaction, which increases its permeability. This dynamic change in the fabric permeability influences the resin flow patterns. Thus, the compaction of the fabric preform and the mould filling physics are coupled. Analysis of this behaviour allows us to conclude that the use of the same infusion flow direction the final thickness of the composite part do not depend on the

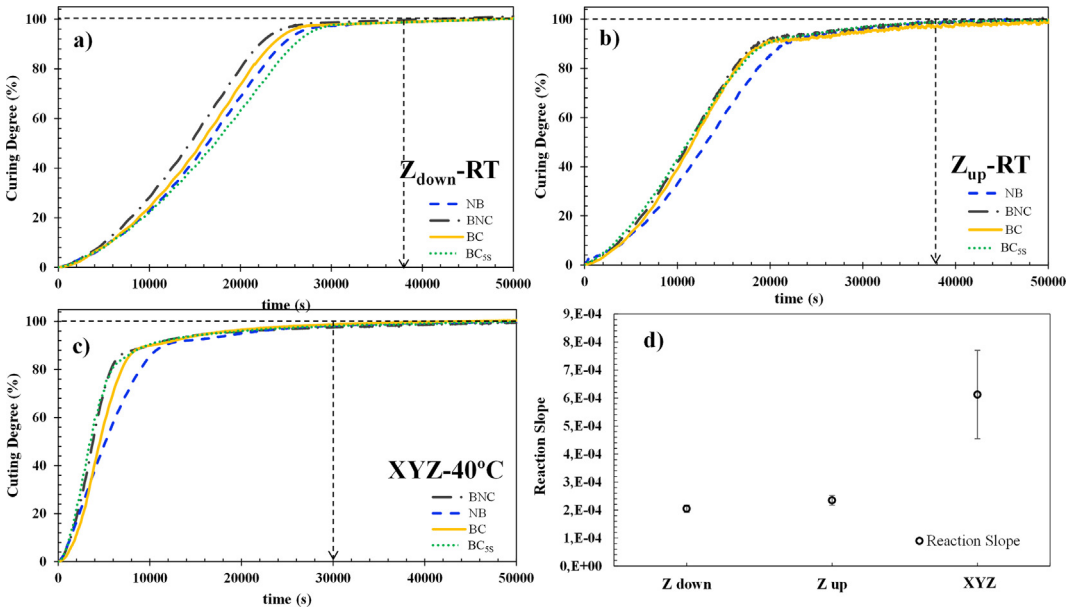

Fig. 9 – Curing degree versus time for all studied laminates (NB, BNC, BC, and BC_{5S}) at 1 Hz for a) Z_{down} and b) Z_{up} and c) XYZ infusions. d) Reaction slope versus type of flow direction. Error bars represent the standard deviation for each laminate configuration.

previous compaction process, and the presence of the binder does not affect the thickness, as long as it is melted. Comparing the flow directions used in the infusion process, the minimum thickness variation was obtained when Z_{down} flow was used.

From a manufacturing point of view, direct lamination of unbindered NCFs, for no complex geometries, will result in a cost-effective process in that the fibres can settle directly under the vacuum bag, thus saving time and energy.

3.2.3. *Fibre volume fraction*

The fibre volume fraction (FVF), void content, and thicknesses of the different composite parts are shown in Fig. 11. The manufactured composite parts, that is, five samples of each laminate group, were gathered depending on the resin infusion flow direction.

Z_{down} resin infusion displays little deviation from the nominal fraction of 60% [57], which was set as the nominal acceptance threshold for many carbon composite

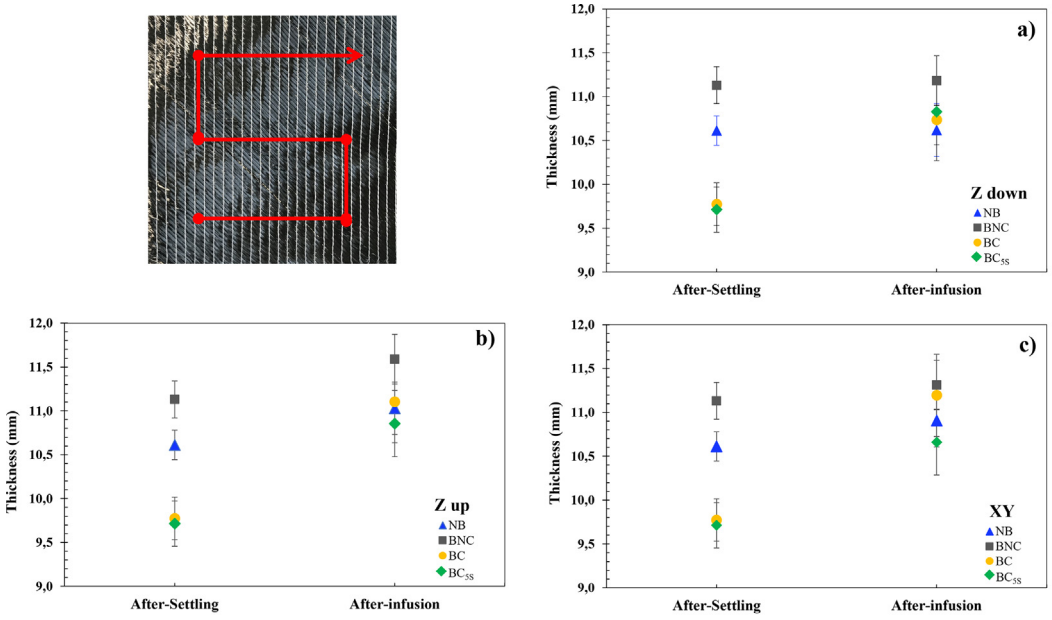

Fig. 10 – Upper Left: Thickness pattern laser measurement. Thickness results for all infused laminates (NB, BNC, BC, and BC_{5S}) in the Z_{down} (a), Z_{up} (b), and XYZ (c) flows, before (after settling) and after infusion.

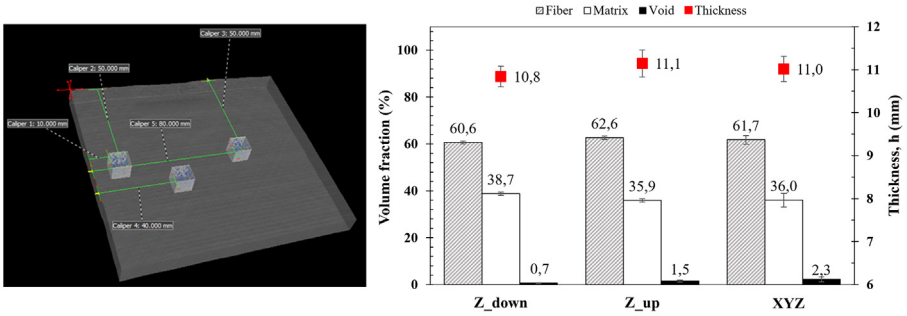

Fig. 11 – Left panel: Selected regions for acid digestion. Right panel: Composite final thickness and fibre, matrix, and void content as determined by acid digestion for each composite part and resin infusion configuration (Z_{down}, Z_{up}, and XYZ). Error bars correspond to the dispersion among NB, BNC, BC, and BC_{5S} in each resin flow direction.

components. Higher FVF, porosity values, and thicknesses were obtained for the Z_{up} and XYZ resin infusion flow directions. Excess FVF decreases the mechanical properties of the composite owing to the lack of space for the matrix to fully embed and bond with the fibres [58]. In this case, not only are the FVF of the Z_{up} and XYZ flows higher, but also the dimensional analysis of composite parts has higher thicknesses, which indicates that the manufacturing processes lead to the formation of voids, as can be observed in the void content results. In other words, thicker laminates have to present a lower FVF, because more resin infiltrates into the preform, whereas in this case, there is a greater thickness but a higher FVF. This points to the porosity of the composite part. In accordance with the literature [59], higher fibre contents and larger porosities are related to the rapid flow of the resin in the infusion process, which generates cavities (inter-tow and intra-tow porosity) throughout the thickness of the sample. High levels of porosity in composite materials have been recognised as a serious problem, with a figure of 2% being accepted as the nominal acceptance threshold for many composite components [60,61]. Nevertheless, it must be considered that acid digestion of the different samples was performed on a small sample (dimensions, 10 × 10 mm, Fig. 11) over the entire composite part. Hence, the experimental results obtained from acid digestion were extracted from discrete portions of the composite parts, which might not be representative of the entire sample volume. X-ray computed tomography (CT) was used to obtain more comprehensive information on the internal structures of the fabricated parts.

3.2.4. *X-ray computed tomography (CT)*

Defect analysis of the samples can be automatically carried out due to each voxel having a grey value intensity that corresponds to the material density [62]. To quantitatively determine the volume and distribution of the pores, the VGEasyPore defect detection algorithm was used. This algorithm is based on the relative or absolute definition of the minimum local contrast of the pores. All the porosity analyses were performed using the VGEasyPore algorithm. This approach identifies regions as defects based on the local grey value of the material in relation to a specified local contrast threshold and can detect defects that are connected to the surrounding air. In contrast to the other defect detection algorithms, the VGEasyPore algorithm provides the possibility of calculating certain defect properties with subvoxel accuracy [63].

The objective of this analysis is to complete the results of porosity obtained by acid digestion by analysing the dispersion of the porosity over the volumes of the samples. First, each sample was scanned as a whole. Subsequently, two regions of interest (ROIs) were defined for each sample to obtain both porosity relative values and deviations.

Figure 12 shows computed tomography (CT) images of the manufactured NCF composite parts where a general view of the scattering and location of all the pores can be seen. The pores are highly heterogeneously distributed through the volumes of all the samples. For defect segmentation, the VGEasyPore algorithm was applied in relative mode, which determines the regions that belong to a defect on the basis of a relative contrast threshold (percentage of the material grey value). The selected value was 20%, which means that all those zones with a contrast difference greater than 20% compared to their surroundings are considered to be defects.

Furthermore, the overall closing option was selected, which allows us to include defects that are separated by the determined surface from the material. The air grey value was automatically selected. To specify the search area around each voxel for determining the contrast, the local area size was adjusted to 10 voxels [64].

From a qualitative point of view, the 3D-CT views show that the porosity is highly heterogeneously distributed over the horizontal plane, which cannot be detected by acid digestion. Moreover, in the CT cross-sectional images, the detected pores are located depending on the resin-feeding strategy, as shown in Fig. 3. In both the Z_{down} and Z_{up} flow directions, pores were located according to the resin inlet configuration. In the XYZ-infused samples, the pores are more homogeneously distributed and mainly located in the middle of the part, in line with the resin pathway in the in-plane direction. Figure 13 shows detailed CT images of an ROI for a BC sample. The porosity is mainly located in the centre of the sample, specifically, in the part of the resin, as shown by the circles drawn following the fibre directions.

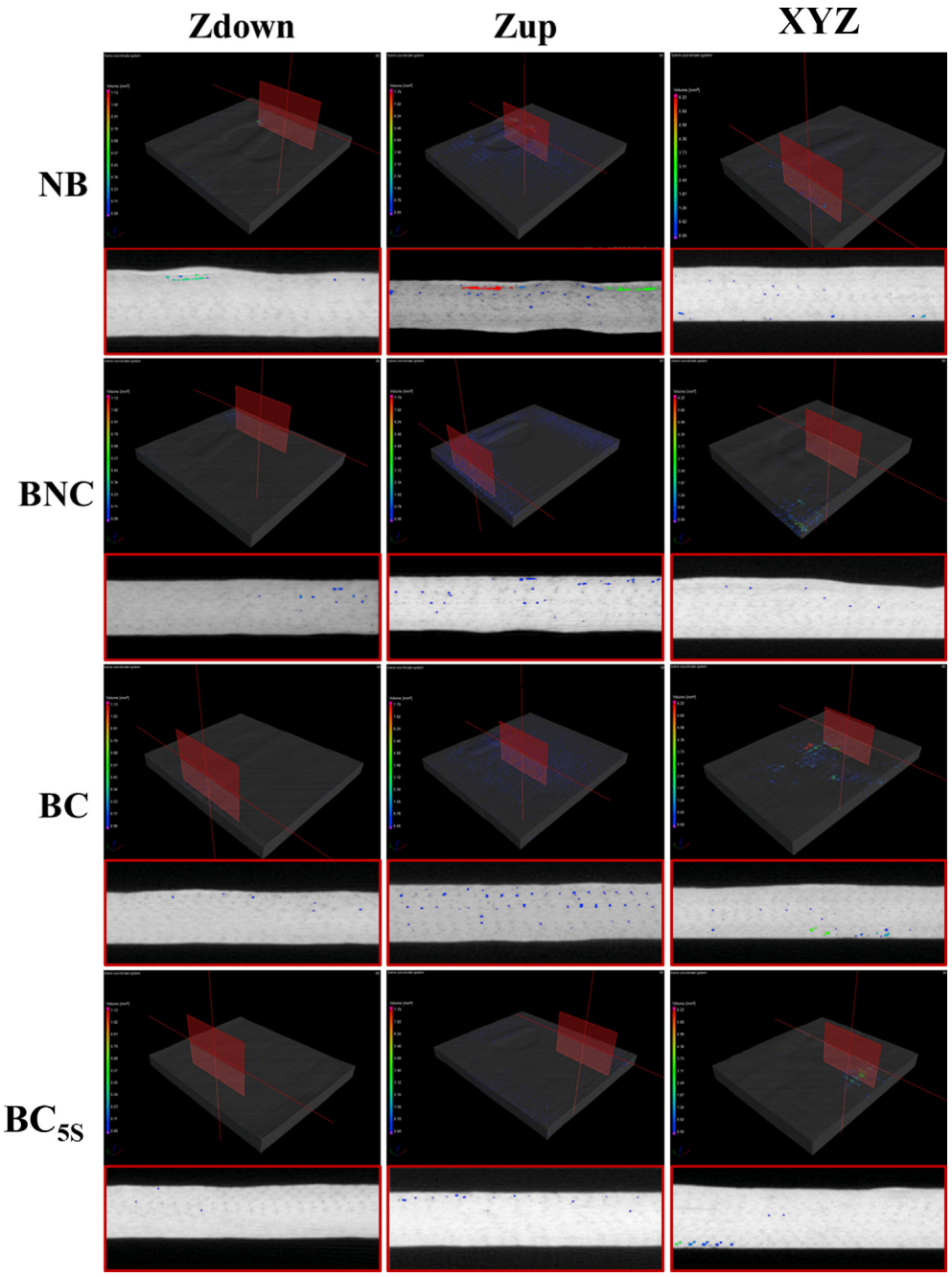

Fig. 12 – Examples of different porosity distributions in all laminates for the three studied flow directions. In the examples, each laminate is viewed as a 3D angled view and the corresponding CT slice image (below). In each CT slice, the detected porosity is highlighted in blue.

From a quantitative point of view, and to better interpret the number of pores present in each studied sample, Fig. 14 represents the pore distribution diagrams for a given volume of each manufactured composite.

Note that the porosity distributions in the samples are not homogeneous; therefore, analysing each sample as a whole, the porosity distributions seem to be coherent with the acid digestion results, resulting in Zdown composite parts having lower pore distributions over the full volume.

To determine the porosity heterogeneity along the horizontal plane, ROI 1 and ROI 2, described in Fig. 15, were defined by analysing the 2-mm thickness of the top and bottom surfaces of the composite parts.

The numerical results, calculated according to Eqs. (3) and (4) are shown in Fig. 16, where the mean value of porosity obtained from both ROI 1 and ROI 2 is normalised for each sample. The porosity distribution was provided by the standard deviation.

$$Mean\ value(\%) = \frac{x_i - \overline{x}}{\overline{x}} \cdot 100 \quad (3)$$

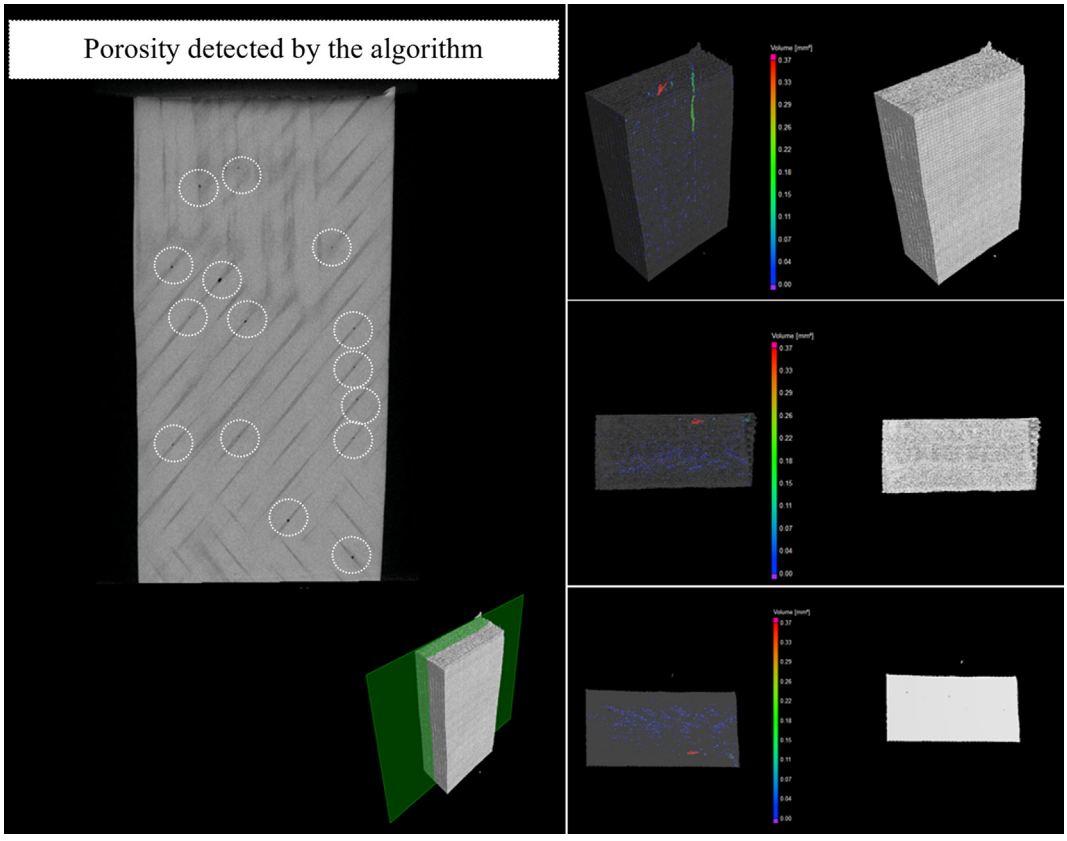

Fig. 13 – Example of one of the two regions of interest (ROIs) defined in each sample to obtain both porosity relative values and deviations. The example ROI belongs to a BC sample manufactured with XYZ infused direction. The porosity distribution can be observed. On the right, three different views are shown (transparency and opacity) – from the top to the bottom: 3D view, top view, and bottom view.

$$Standard\ deviation(\%) = \frac{1}{\overline{x}} \cdot \sqrt{\frac{\sum_{i=1}^{N}(x_i - \overline{x})^2}{N-1}} \cdot 100 \quad (4)$$

Deviation values up to 140% can be found in the Z_{up}, Z_{down}, and XYZ infused directions. Moreover, in line with the qualitative results, the porosity level for the Z_{up} configuration is mostly located in the lower part of the infused laminate, whereas for Z_{down}, the pores are mainly in the upper part of the sample, following the resin inlet lines. The XYZ infused flow direction appears to produce the most homogenous pattern in terms of porosity distribution, namely, in the NB and BNC samples, owing to the lack of hindrance resulting from the previous dry laminate compaction step. The porosity difference between the Z-direction and XYZ flow configurations can be explained by the internal air being evacuated during the infusion process. In the Z-direction, the air is evacuated through the semipermeable membrane, where the generated volatiles escape through the membrane layer. Nevertheless, because of the rapid resin infusion observed in the Z_{up} flow direction, cavities (inter-tow and intra-tow porosity) [59] were generated throughout the thickness of the sample.

4. Summary and conclusions

In this study, the effects of carbon fibre laminate preforming, resin infusion direction, and porosity distribution in the manufacturing process were evaluated by dimensional analysis, dielectric analysis, acid digestion, and X-ray computed tomography (CT). The porosity distribution was detected by CT tests conducted on resin-infused samples and quantified using the VGStudio MAX software. Given the results of this study, the following conclusions can be drawn:

- The forming results show that carbon non-crimp fabric (NCF) laminates are more compressed in the settling step because fibres and tows slide into each other and stack more freely, creating a nesting effect, and the deformation behaviour is mainly viscous. Regardless of the number of compaction steps to which the laminates are subjected, as long as the binder activation temperature is overcome under vacuum pressure, fully compressed laminates are obtained. The settling stage defines the steady-state

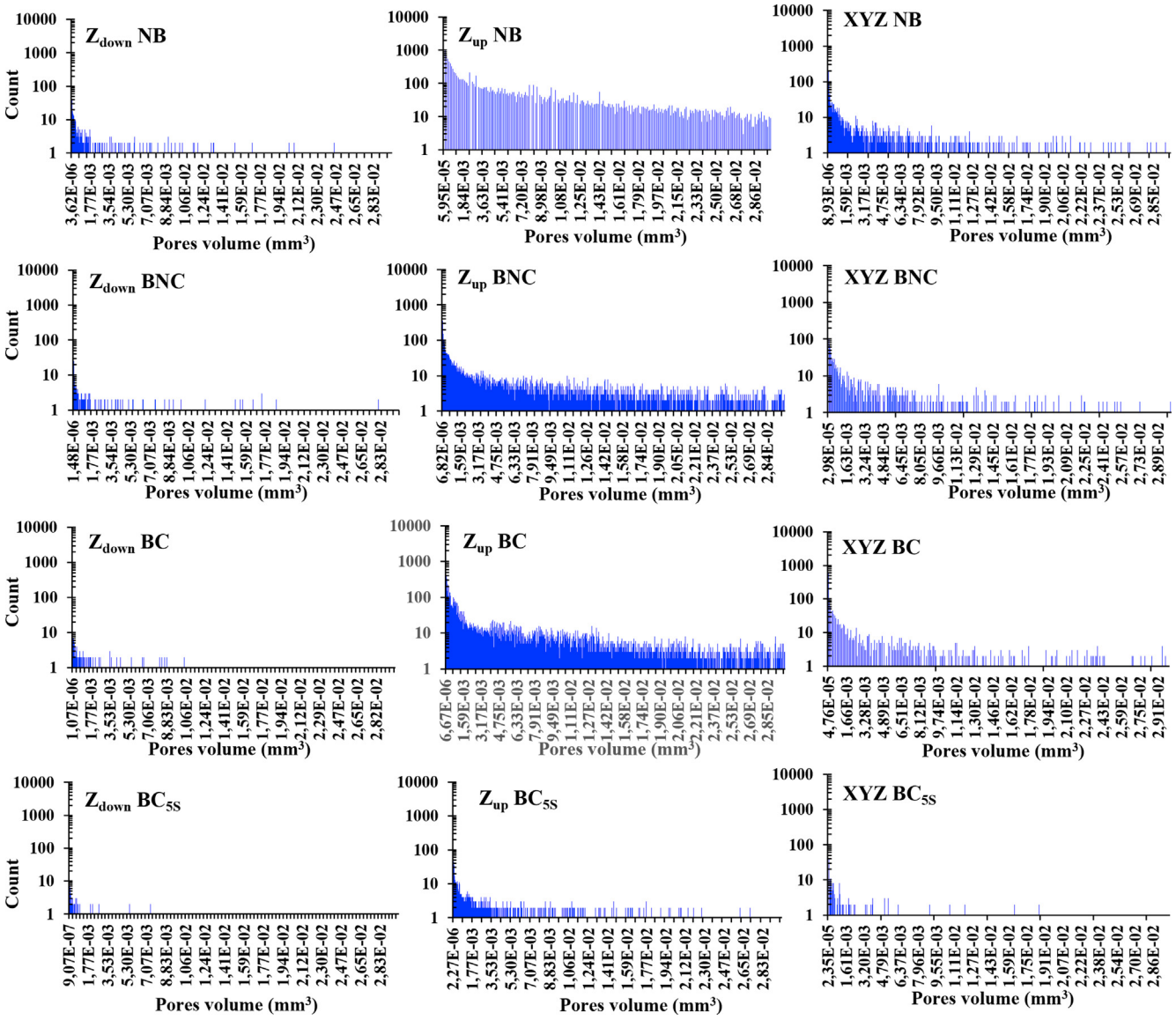

Fig. 14 – Defect volume distribution diagrams. Pores with a volume up to 0.03 mm³ have been included to enable a more direct comparison between the different porosity levels.

specimen thickness, which was set as the initial thickness before resin infusion of dry NCF laminates.

- The "effective" permeability in the in-plane XYZ direction of all the studied laminates is lower than that in the Z direction, even when infusing the resin at 40 °C. The unbindered (NB) and bindered but not compacted (BNC) samples exhibit a higher permeability in the Z_{up} flow direction as a consequence of the different configurations set in the Z_{down} and Z_{up} flows. The placement of the distribution mesh influences the functionality. In the Z_{down} configuration, the distribution mesh is in contact with the vacuum bag, which could lead to the penetration of the vacuum bag into the unit cells of the distribution mesh under external pressure. This penetration changes the overall "effective" permeability of the system. In the Z_{up} configuration, the distribution mesh is in direct contact with a rigid surface, and its functionality remains unchanged. This effect does

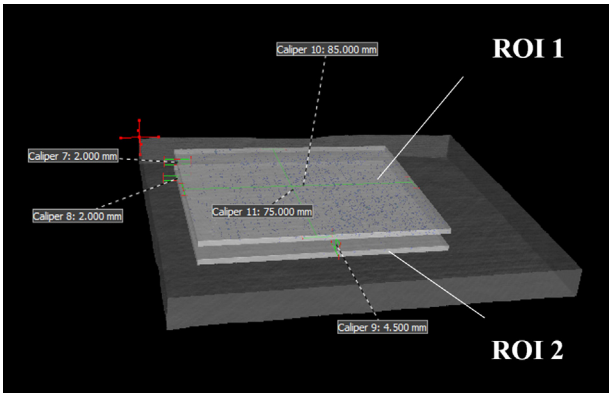

Fig. 15 – ROI 1 and ROI 2 definition for each manufactured composite part.

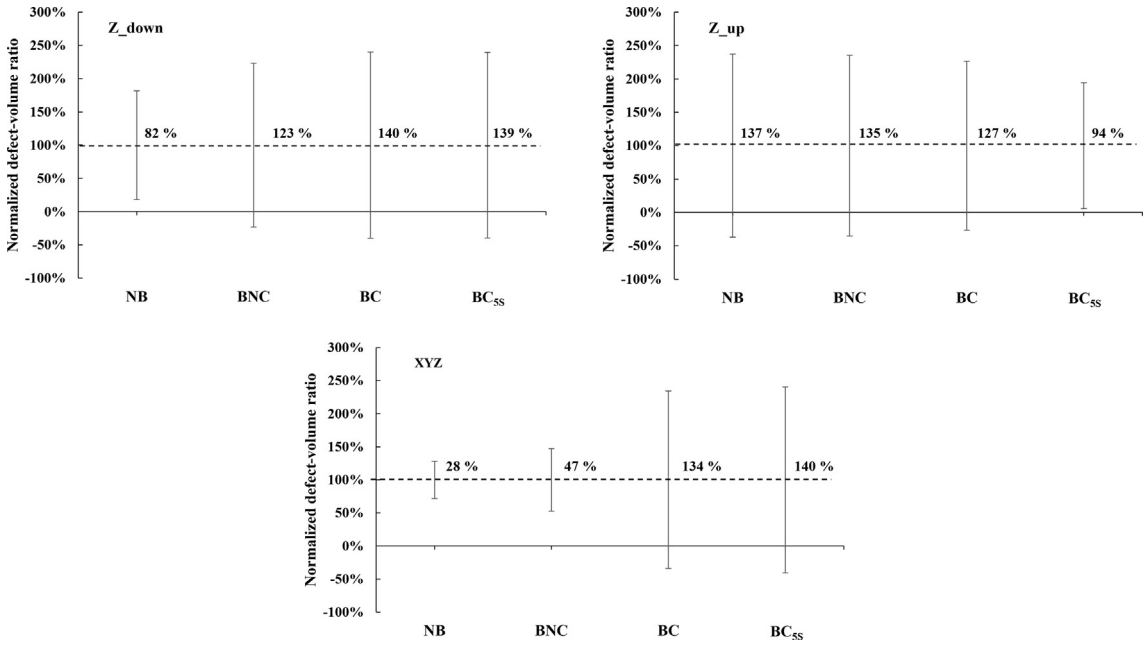

Fig. 16 – Mean porosity and standard deviation percentage for ROI 1 and ROI 2 in each sample.

not occur when comparing BC and BC_{5S} laminates in the Z_{down} and Z_{up} flows because of the lower permeability of the compacted laminates. The results show that the composite parts manufactured using the Z_{down} configuration have the lowest thickness values.

- Characterisation techniques such as acid digestion and X-ray tomography allow the assessment of the quality of the composite parts. This last technique makes it possible to visualise the porosities in composite parts with different resin-filling strategies. The through-thickness downward infusion, Z_{down}, presents benefits through the evacuation of air/volatiles and thickness tolerances of the final composite parts. Regarding the heterogeneity of the infused samples, deviation values of up to 140% were found in the Z_{down}, Z_{up}, and XYZ infused directions. For the Z-direction resin infusion strategies, most of the pores were located on the surface of the composite parts. In the in-plane XYZ infused flow direction, the porosity distribution is more homogenous in NB and BNC laminate configurations because of the ease with which the resin can flow along the fibres.

Declaration of Competing Interest

The authors declare that they have no known competing financial interests or personal relationships that could have appeared to influence the work reported in this paper.

Acknowledgments

The authors acknowledge the Spanish Government (Ministry of Science and Innovation, Centro para el Desarrollo Tecnológico Industrial (CDTI) program) for their financial support. We thank the Aerostructures Competence Center at the CBC, Airbus Defense & Space, for the advice received on the configuration of the infusion systems, and to Ronand Fiacre of SAERTEX GmbH & Co. KG for supplying the carbon NCF material.

REFERENCES

[1] Falzon BG, Pierce RS. Thermosetting composite materials in aerostructures. In: Pantelakis S, Tserpes K, editors. Revolutionizing aircraft materials and processes. Cham: Springer International Publishing; 2020. p. 57–86. https://doi.org/10.1007/978-3-030-35346-9_3.

[2] Large, high-volume, infused composite structures on the aerospace horizon. Composites World 2019. https://www.compositesworld.com/articles/large-high-volume-infused-composite-structures-on-the-aerospace-horizon. [Accessed 21 December 2020].

[3] Miracle DB, Donaldson SL. ASM handbook composites, vol. 21. ASM International; 2004.

[4] Lomov SV, editor. Non-crimp fabric composites manufacturing, properties and applications. 1st ed. Woodhead Publishing; 2011.

[5] Rufe PD. Fundamentals of manufacturing. ed. Society of Manufacturing Engineers; 2013.

[6] Linke M, Greb C, Klingele J, Schnabel A, Gries T. 9 - automating textile preforming technology for mass production of fibre-reinforced polymer (FRP) composites. In: Shishoo R, editor. The global textile and clothing industry. Woodhead Publishing; 2012. p. 171–95. https://doi.org/10.1533/9780857095626.171.

[7] Helber F, Amann A, Carosella S, Middendorf P. Intrinsic fibre heating: a novel approach for automated dry fibre placement. IOP Conf Ser Mater Sci Eng 2018;406:012064. https://doi.org/10.1088/1757-899X/406/1/012064.

[8] Buelga-Sánchez R, Moreno-Diaz JA, Rubio-García L. Automation of dry fibre composites materials: current state and future possibilities. SAMPE Conference Southampton; 2018. p. 7.
[9] Fauster E, Schillfahrt C, Hueber C, Schledjewski R. Automated profile preforming for structural components. Sci Eng Compos Mater 2017;24:631–50. https://doi.org/10.1515/secm-2015-0377.
[10] Kruijk JC de. Automated composite manufacturing using robotics lowers cost, lead-time and scrap rate. Netherlands Aerospace Centre NLR; 2018.
[11] Proving viability of dry fabrics, infusion for large aerostructures. Composites World 2019. https://www.compositesworld.com/articles/proving-viability-of-dry-fabrics-infusion-for-large-aerostructures. [Accessed 9 December 2021].
[12] Dry fiber placement: surpassing limits. Composites World. 2016. https://www.compositesworld.com/blog/post/dry-fiber-placement-surpassing-limits. [Accessed 5 June 2020].
[13] Matveev MY, Schubel PJ, Long AC, Jones IA. Understanding the buckling behaviour of steered tows in automated dry fibre placement (ADFP). Compos Appl Sci Manuf 2016;90:451–6. https://doi.org/10.1016/j.compositesa.2016.08.014.
[14] Breuer UP. Commercial aircraft composite technology. 1st ed. Springer International Publishing; 2016.
[15] Khan LA, Mehmood AH. 5 - cost-effective composites manufacturing processes for automotive applications. In: Njuguna J, editor. Lightweight composite structures in transport. Woodhead Publishing; 2016. p. 93–119. https://doi.org/10.1016/B978-1-78242-325-6.00005-0.
[16] Lunn P. Cost-effective resin infusion. Reinforc Plast 2009;53:38–9. https://doi.org/10.1016/S0034-3617(09)70047-5.
[17] Summerscales J. Resin infusion under flexible tooling (RIFT). Wiley Encyclopedia of Composites, American Cancer Society; 2012. p. 1–11. https://doi.org/10.1002/9781118097298.weoc216.
[18] Kazmi S, Govignon Q, Bickerton S. Control of laminate quality for parts manufactured using the resin infusion process. J Compos Mater 2018:1–17. https://doi.org/10.1177/0021998318783308.
[19] Grimsley BW, Cano RJ, Hubert P, Loos AC, Kellen CB, Jensen BJ. Preform characterization in VARTM process model development. In: 36th international SAMPE technical conference; 2004.
[20] Yenilmez B, Senan M, Murat Sozer E. Variation of part thickness and compaction pressure in vacuum infusion process. Compos Sci Technol 2009;69:1710–9. https://doi.org/10.1016/j.compscitech.2008.05.009.
[21] Yenilmez B, Sozer EM. Compaction of e-glass fabric preforms in the vacuum infusion process. A: Character Exp Comp Part A: App Sci Manuf 2009;40:499–510. https://doi.org/10.1016/j.compositesa.2009.01.016.
[22] Yenilmez B, Sozer EM. Compaction of e-glass fabric preforms in the vacuum infusion process: (a) use of characterization database in a model and (b) experiments. J Compos Mater 2013;47:1959–75. https://doi.org/10.1177/0021998312453075.
[23] Yenilmez B, Caglar B, Sozer EM. Pressure-controlled compaction characterization of fiber preforms suitable for viscoelastic modeling in the vacuum infusion process. J Compos Mater 2017;51:1209–24. https://doi.org/10.1177/0021998316685164.
[24] Niggemann C, Song YS, Gillespie JW, Heider D. Experimental investigation of the controlled atmospheric pressure resin infusion (CAPRI) process. J Compos Mater 2008;42:1049–61. https://doi.org/10.1177/0021998308090650.
[25] Kim YR, McCarthy SP, Fanucci JP. Compressibility and relaxation of fiber reinforcements during composite processing. Polym Compos 1991;12:13–9. https://doi.org/10.1002/pc.750120104.
[26] Aranda S, Klunker F, Ziegmann G. Compaction response of fibre reinforcements depending on processing temperature. 2009. p. 10.
[27] Aranda S, Klunker F, Ziegmann G. Influence of the binding system on the compaction behaviour of NCF carbon fibre reinforcements. 2011. p. 6.
[28] Wei K, Liang D, Mei M, Wang D, Yang X, Qu Z. Preforming behaviors of carbon fiber fabrics with different contents of binder and under various process parameters. Compos B Eng 2019;166:221–32. https://doi.org/10.1016/j.compositesb.2018.11.143.
[29] Seemann WH. Plastic transfer molding techniques for the production of fiber reinforced plastic structures. 1990. US4902215A.
[30] Woods JA, Modin AE, Hawkins RD, Hanks DJ. Controlled atmospheric pressure resin infusion process. 2008. US7334782B2.
[31] Hou T-H, Jensen BJ. Double vacuum bag process for resin matrix composite manufacturing. 2007. US7186367B2.
[32] Vernin N, Chohra M, Advani S, Alms J. Vacuum assisted resin transfer molding techniques with flow flooding chamber. 2007. WO2007040797A2.
[33] Wilson RS, Braniff MA, Millar WJT. A bagging blanket and method for forming a fibre reinforced resin composite component. GB2316036B.
[34] VAP® patent. http://www.vap.trans-textil.de/vap_patent_en.html (accessed June 5, 2019).
[35] Li W, Krehl J, Gillespie JW, Heider D, Endrulat M, Hochrein K, et al. Process and performance evaluation of the vacuum-assisted process. J Compos Mater 2004;38:1803–14. https://doi.org/10.1177/0021998304044769.
[36] Hindersmann A. Confusion about infusion: an overview of infusion processes. Compos Appl Sci Manuf 2019;126:105583. https://doi.org/10.1016/j.compositesa.2019.105583.
[37] Li C, Fu Y, Wang B, Zhang W, Bai Y, Zhang L, et al. Effect of pore structure on mechanical and tribological properties of paper-based friction materials. Tribol Int 2020;148:106307. https://doi.org/10.1016/j.triboint.2020.106307.
[38] Jiming Z, Wuqiang Z, Lehua Q, Yuqin M, Xinliang W, Yuanbiao Z. Fabrication of PyC/SiC compound coating on carbon fiber preform and its effect on the properties of Cf/Al composite. Rare Met Mater Eng 2015;44:1851–6. https://doi.org/10.1016/S1875-5372(15)30112-0.
[39] sicomin.com/datasheets n.d. http://www.sicomin.com/datasheets/product-pdf94.pdf.
[40] Li L, Zhao Y, Yang J, Zhang J, Duan Y. An experimental investigation of compaction behavior of carbon non-crimp fabrics for liquid composite molding. J Mater Sci 2015;50:2960–72. https://doi.org/10.1007/s10853-015-8860-0.
[41] Runt JP, Fitzgerald JJ. Dielectric spectroscopy of polymeric materials: fundamentals and applications. American Chemical Society; 1997.
[42] ASTM D3171-15. Standard test methods for constituent content of composite materials. 2016. https://www.astm.org/d3171-15.html. [Accessed 31 January 2022].
[43] UNE EN ISO 1183-1:2019 Plastics - Methods for determining the density of non-cellular plastics. https://www.en-standard.eu/une-en-iso-1183-1-2019-plastics-methods-for-determining-the-density-of-non-cellular-plastics-part-1-immersion-method-liquid-pycnometer-method-and-titration-method-iso-1183-1-2019-corrected-version-2019-05/ (accessed January 31, 2022).
[44] UNE EN 2564:2018 Aerospace series. Carbon fibre laminates. Determination of the fibre, resin and void contents (accessed January 31, 2022).
[45] Wu W, Jiang B, Xie L, Klunker F, Aranda S, Ziegmann G. Effect of compaction and preforming parameters on the compaction behavior of bindered textile preforms for

automated composite manufacturing. Appl Compos Mater 2013;20:907–26. https://doi.org/10.1007/s10443-012-9308-1.
[46] Gupta N, Sundaram R. Fiber optic sensors for monitoring flow in vacuum enhanced resin infusion technology (VERITy) process. Compos Appl Sci Manuf 2009;40:1065–70. https://doi.org/10.1016/j.compositesa.2009.04.022.
[47] Wang P, Molimard J, Drapier S, Vautrin A, Minni JC. Monitoring the resin infusion manufacturing process under industrial environment using distributed sensors. J Compos Mater 2012;46:691–706. https://doi.org/10.1177/0021998311410479.
[48] Antonucci V, Giordano M, Nicolais L, Calabrò A, Cusano A, Cutolo A, et al. Resin flow monitoring in resin film infusion process. J Mater Process Technol 2003;143–144:687–92. https://doi.org/10.1016/S0924-0136(03)00338-8.
[49] Hancioglu M, Sozer EM, Advani SG. Comparison of in-plane resin transfer molding and vacuum-assisted resin transfer molding 'effective' permeabilities based on mold filling experiments and simulations. J Reinforc Plast Compos 2020;39:31–44. https://doi.org/10.1177/0731684419868015.
[50] Rohatgi V, Lee LJ. Moldability of tackified fiber preforms in liquid composite molding. J Compos Mater 1997;31:720–44. https://doi.org/10.1177/002199839703100705.
[51] Chen J, Backes D, Jayaraman K. Dynamics of binder displacement in liquid molding. Polym Compos 1996;17:23–33. https://doi.org/10.1002/pc.10587.
[52] Zhang Y, Lopatnikov S, Heider D. Modeling of distribution media and vacuum bag properties on permeability variations during vacuum assisted resin transfer molding (VARTM). American Society of Mechanical Engineers Digital Collection; 2008. p. 1177–84. https://doi.org/10.1115/IMECE2005-82732.
[53] Drapier S, Pagot A, Vautrin A, Henrat P. Influence of the stitching density on the transverse permeability of non-crimped new concept (NC2) multiaxial reinforcements: measurements and predictions. Compos Sci Technol 2002;62:1979–91. https://doi.org/10.1016/S0266-3538(02)00127-6.
[54] Raponi O de A, Raponi R de A, Barban GB, Benedetto RMD, Ancelotti Junior AC, Raponi O de A, et al. Development of a simple dielectric analysis module for online cure monitoring of a commercial epoxy resin formulation. Mater Res 2017;20:291–7. https://doi.org/10.1590/1980-5373-mr-2017-0067.
[55] Lionetto F, Moscatello A, Maffezzoli A. Effect of binder powders added to carbon fiber reinforcements on the chemoreology of an epoxy resin for composites. Compos B Eng 2017;112:243–50. https://doi.org/10.1016/j.compositesb.2016.12.031.
[56] Helber F, Szcesny M, Carosella S, Middendorf P. Enhancement on automated preforming dor composite structures. 2019.
[57] Chung DDL. 3 - polymer-matrix composites: structure and processing. In: Chung DDL, editor. Carbon composites. ed. Butterworth-Heinemann; 2017. p. 161–217. https://doi.org/10.1016/B978-0-12-804459-9.00003-8.
[58] Pantelakis S, Tserpes K, editors. Revolutionizing aircraft materials and processes. Springer International Publishing; 2020. https://doi.org/10.1007/978-3-030-35346-9.
[59] Bodaghi M, Lomov SV, Simacek P, Correia NC, Advani SG. On the variability of permeability induced by reinforcement distortions and dual scale flow in liquid composite moulding: a review. Compos Appl Sci Manuf 2019;120:188–210. https://doi.org/10.1016/j.compositesa.2019.03.004.
[60] Bossi RH, Giurgiutiu V. 15 - nondestructive testing of damage in aerospace composites. In: Irving PE, Soutis C, editors. Polymer composites in the aerospace industry. Woodhead Publishing; 2015. p. 413–48. https://doi.org/10.1016/B978-0-85709-523-7.00015-3.
[61] Birt EA, Smith RA. A review of NDE methods for porosity measurement in fibre-reinforced polymer composites. Insight - Non-Destructive Test Cond Monitor 2004;46:681–6. https://doi.org/10.1784/insi.46.11.681.52280.
[62] Villarraga-Gómez H, Herazo EL, Smith ST. X-ray computed tomography: from medical imaging to dimensional metrology. Precis Eng 2019;60:544–69. https://doi.org/10.1016/j.precisioneng.2019.06.007.
[63] VolumeGraphics VGStudio MAX 3.4 reference manual, Section 29, p. 560.
[64] What's New in VGSTUDIO MAX 3.4.x. Industrial CT Software | Volume Graphics. https://www.volumegraphics.com/en/products/vgsm/what-s-new-in-vgstudio-max-3-4-x.html (accessed October 21, 2021).